Volatile evolution and atmospheres of Trans-Neptunian Objects

Leslie A. Young[a]

Felipe Braga-Ribas[b]

Robert E. Johnson[c]

[a] *Southwest Research Institute, Boulder CO, USA*
[b] *Federal University of Technology - Paraná/Brazil - UTFPR/Curitiba*
[c] *University of Virginia, Charlottesville, VA, USA*

Abstract

At 30-50 K, the temperatures typical for surfaces in the Kuiper Belt (e.g. Stern & Trafton 2008), only seven species have sublimation pressures higher than 1 nbar (Fray & Schmitt 2009): Ne, N_2, CO, Ar, O_2, CH_4, and Kr. Of these, N_2, CO, and CH_4 have been detected or inferred on the surfaces of Trans-Neptunian Objects (TNOs). The presence of tenuous atmospheres above these volatile ices depends on the sublimation pressures, which are very sensitive to the composition, temperatures, and mixing states of the volatile ices. Therefore, the retention of volatiles on a TNO is related to its formation environment and thermal history. The surface volatiles may be transported via seasonally varying atmospheres and their condensation might be responsible for the high surface albedos of some of these bodies. The most sensitive searches for tenuous atmospheres are made by the method of stellar occultation, which have been vital for the study of the atmospheres of Triton and Pluto, and has to-date placed upper limits on the atmospheres of 11 other bodies. The recent release of the Gaia astrometric catalog has led to a "golden age" in the ability to predict TNO occultations in order to increase the observational data base.

Keywords: Trans Neptunian objects, Kuiper Belt Objects, ices, atmospheres

1. Spectral evidence of N_2, CO, and CH_4 on the surfaces of TNOs

Methane ice has been reported or inferred on the surfaces Triton, Pluto, Eris, Makemake, Quaoar, Varuna, Sedna, and 2007 OR_{10}. CO and N_2 ices have been directly detected on Pluto and Triton. N_2 ice has been inferred from its effect on the CH_4-dominated spectra of Eris and Makemake, and possibly Quaoar and Sedna. We detail the evidence for the presence of such ices below and summarize it in Table 1. See deBergh et al 2013, Brown 2008, 2012, and Grasset et al. 2017 for earlier reviews, and the chapter by Barucci and Merlin for more general discussion of the composition of TNO surfaces. Despite attempts to characterize surfaces compositions with photometric systems (Trujillo et al. 2011, DalleOre et al. 2015), spectral resolution of at least 500 seems to be needed for definitive detections of volatile ices, and we focus on spectral data below.

We consider Triton in the discussion of volatiles on Trans Neptunian Objects, even though it is a moon of Neptune, because it is thought to be a captured TNO (McKinnon & Leith 1995). and, more frivolously, its orbit clearly crosses that of Neptune. Its surface and atmospheric properties are usefully compared to those of Pluto and other large TNOs. The volatiles, N_2 and CH_4, were measured in Triton's atmosphere by Voyager during its 1989 flyby with its UV spectrometer (Broadfoot et al. 1989). Three relatively volatile ices, N_2, CH_4, and CO, and two non-volatile ices, CO_2 and H_2O, were detected on Triton's surface from ground-based near-IR spectroscopy (Cruikshank et al. 1993, Cruikshank et al. 2000). Noting that the spectral profile of the 2.15-μm N_2 absorption band is temperature dependent, and transitions from very broad for the higher-temperature hexagonal β-N_2 phase above 35.61 K to very narrow for the colder cubic α-N_2 phase, Quirico et al. (1999) showed that the N_2 ice was in the warmer β phase on Triton. Additionally, the spectrum of CH_4 ice diluted in N_2 is shifted toward shorter wavelengths with respect to pure CH_4 ice (Quirico & Schmitt 1997). Therefore it was concluded that solid CH_4 on Triton exists predominantly diluted in N_2 (Quirico et al. 1999). These ices are not uniformly distributed across its surface, as seen from the variation of Triton's spectrum with sub-observer longitude as the body rotates (Grundy & Young 2004, Grundy et al. 2010, Holler et al. 2016). These studies suggest that the non-volatiles H_2O and CO_2 may dominate the terrains nearest Triton's current summer pole, that the more volatile species, N_2 and CO, are co-located, that the CH_4 distribution and mixing state may vary with depth and longitude, and that there may be some areas of CH_4 diluted in fine-grained N_2 where the N_2 is revealed only by its effect of shifting the CH_4 spectrum, rather than by a direct detection of the inherently weak 2.15 μm N_2 band. Voyager flew no infrared spectrometer, and so it is likely that these speculations will remain unconfirmed until a mission to Neptune/Triton can fly an infrared spectrometer.

Pluto's surface has been studied with disk-integrated ground-based spectra in the visible, near infrared and mid infrared (see the review by Cruikshank et al. 2015) and at geologically relevant spatial scales by the LEISA infrared spectrometer and MVIC color imager on NASA's New Horizons spacecraft (see chapter by Spencer et al.). The N_2 ice on Pluto is concentrated in a large, deep, N_2-filled basin called Sputnik Planitia, near the equator opposite Charon, in which some CO and CH_4 is diluted in solid solution with large-grained or annealed β-N_2. N_2-rich ice of similar composition is also seen at mid latitudes, 35-55° N (Protopapa et al. 2017; Schmitt et al. 2017). It is now understood that Pluto has more CH_4 than Triton overall. Areas of CH_4-rich ice was first inferred from ground-based spectra, and were mapped with the LEISA spectrometer to be predominately (i) at a northern cap, north of ~55°N, (ii) in a band from 20-35°N, and (iii) on the area named Tartarus Dorsae at low latitude on the eastern terminator limb on the encounter hemisphere.

The visible and near-infrared spectrum of Eris clearly shows strong CH_4 absorption features (Brown et al 2005; see review by Brown 2008 and analysis by Tegler et al. 2012). Absorption at 1.684 μm indicates pure CH_4 or CH_4-rich ice (Dumas et al. 2007), and the spectral shifts are much smaller than for either Triton or Pluto spectra. The depth, shape, and the precise wavelengths of the CH_4 features on Eris can be modeled to derive grain size, dilution state, and stratification of CH_4 ice, even without the direct detection of the N_2 feature (e.g., Merlin et al. 2009). The issue of stratification—i.e., whether the CH_4 concentration state is constant or varying with depth—is particularly interesting because it relates to the evolution of Eris's ices over its 561-year orbit, which in turn is determined by the order in which different species freeze out onto the surface each orbit after perihelion. Different studies have disagreed on the stratification, variously concluding that the dilute CH_4 lies above pure CH_4 (Licardro et al. 2006), below pure CH_4 (Abernathy et al. 2009), sandwiched between two layers of pure CH_4 (Merlin et al. 2009), or that the stoichiometry of CH_4:N_2 is constant with depth (Tegler et al. 2012). Clearly, more work is needed on this question. Eris's surface temperature is almost certainly below the α-β phase transition for N_2 (Sicardy et al. 2011). Since the α-N_2 absorption feature is weaker and much narrower than that of β-N_2, it has eluded direct detection on Eris.

Very strong CH_4 absorption is seen in the visible and infrared spectrum of Makemake with spectral shifts to shorter wavelengths, but with smaller shifts than are seen on Eris, Pluto, or Triton (Licandro et al. 2006, Brown et al. 2007, Tegler et al 2007, 2008, Lorenzi et al. 2015, Perna 2017). This suggests that although some CH_4 is in solution with N_2, N_2 itself is not as prevalent on Makemake as on the previous three bodies. Tegler et al (2007) detected four absorption features between 0.54 to 0.62 μm that they attributed to CH_4, but ice-phase laboratory spectra of these features are lacking.

The spectrum of Quaoar is dominated by H_2O ice, analogous to H_2O-rich Charon. Jewett & Luu (2004) interpreted absorption near 1.65 μm as crystalline water ice and absorption near 2.2 μm as ammonia hydrate, and reported no detected CH_4 absorption. Improved SNR at 2.2-2.4 μm strengthened the case for CH_4 in the spectrum (Schaller & Brown 2007b), which, if real, was nevertheless subtle when superimposed on the significant H_2O absorption. Guilbert et al. (2009) claim a marginal detection (depth 2 ± 2% deep) of the 1.724 μm feature due to CH_4 ice, adding weight to the attribution of CH_4 ice for the 2.2 μm feature. Dalle Ore et al. (2009) model the near-IR spectrum plus photometry at 3.6 and 4.5 μm using CH_4 to explain both the 2.2 μm and the mid-IR photometry, with no need for ammonia hydrate, and propose that N_2 ice in the β-phase may cover 20% of the surface, as seen by relatively subtle effects near 2.15 μm and by photometry at 3.6 and 4.5 μm. Barucci et al. (2015) investigate the 1.67 μm CH_4 band, and N_2 implied by the shifts in the 1.67 μm CH_4 band, but measuring this shift is complicated by the broad 1.65 μm H_2O band. In short, on Quaoar strong H_2O bands complicate the definitive detection and analysis of CH_4, and derived presence of N_2 from CH_4 shifts.

The large TNO 2007 OR_{10} (Pál et al. 2016) shows an extremely red visible spectrum, and its near-IR spectrum shows water-ice absorption (Brown et al. 2011). 2007 OR_{10} shares both traits with Quaoar. This similarity with Quaoar is indirect evidence that CH_4 may also be present on 2007 OR_{10} (Brown et al., 2011), if one accepts both the equivalence of surface type, and the evidence of CH_4 on Quaoar. Both Quaoar and 2007 OR10 are near the CH_4 retention line of Schaller and Brown (2007a), see Section 3.

Distant Sedna, currently at ~85 AU, has a spectrum that is difficult to interpret. Barucci et al. (2005) reported hints of a Triton-like spectrum with N_2 and CH_4, while Trujilo et al. (2005) reported a featureless spectrum. Near-infrared spectra were analyzed in combination with Spitzer photometry at 3.6 and 4.5 μm (Barucci et al. 2010, Emery et al. 2007). No diagnostic CH_4 absorption bands were evident, but a decrease in albedo longward of 2.2 μm was interpreted as due to CH_4 and C_2H_6 (ethane), or possibly serpentine, and the addition of N_2 was also consistent with the Spitzer photometry (Barucci et al., 2010). The surface appears heterogeneous (Barucci et al. 2010).

The spectrum of Varuna is in general well explained by various non-volatiles, such as water ice, olivine, pyroxene, tholin, and amorphous carbon as a darkening agent. The strong CH_4 absorption bands at 1.67, 1.72, 1.8, or 2.21 μm are not detected in the current best spectra (Lorenzi et al. 2014), limiting the amount of CH_4 ice to less than 10% of the surface. However, the addition of CH_4 slightly improves the model fit to the data (Lorenzi et al. 2014). The improvement is particularly evident at 2.3 μm, which is within the last three points near the long-wavelength end of sensitivity in the K band near the edge of the detector. As these data have spectral resolution of only 50, further work is critically needed before to confirm or constrain CH_4 on Varuna.

The water-dominated near-infrared spectrum of Orcus (de Bergh et al. 2005, Fornasier et al. 2004, Trujillo et al. 2005) has an absorption feature near 2.2 μm, compatible with absorption by CH_4, NH_3, or NH_4^+ (Barucci et al. 2008; Delsanti et al. 2010; Carry et al. 2011; DeMeo et al. 2010). Because of the lack of other CH_4 absorptions, specifically those near 1.67 and 1.72 μm, it is likely that CH_4 is not the main cause of the 2.2 μm absorption feature.

INSERT TABLE 1 HERE

2. Volatile-supported atmospheres

For a TNO with little or no atmosphere, the equilibrium surface temperature, T_0 will depend on its rotation regime (i.e. fast or slow rotator), latitude, sub-solar latitude, and time of day. The simplest approach is to assume thermal emission balances absorbed insolation, and that the atmosphere is nearly transparent, in which case the equilibrium surface temperature is:

(1) $$\epsilon\sigma T_0^4 = \overline{\mu(\lambda,\lambda_{sol},h)}\left(\frac{S_{1AU}(1-A)}{\eta R^2}\right)$$

where ϵ is the emissivity, σ is the Stefan–Boltzmann constant, S_{1AU} is the normal solar insolation at 1 AU (1367 W m^{-2}), A is the bolometric Bond albedo, and R is the heliocentric distance in AU. $\overline{\mu(\lambda,\lambda_{sol},h)}$ is the average cosine of the incidence angle for the problem at hand: for the sub-solar temperature on a slow rotator, T_{ss}, $\bar{\mu} = 1$; for the equatorial latitude for fast rotator, $\bar{\mu} = 1/\pi$; for a single characteristic equilibrium temperature balancing the global average of the insolation, T_{eq}, $\bar{\mu} = 1/4$. η is the so-called "beaming parameter" (e.g., Lellouch et al. 2013), which can raise the temperature for a rough surface (or lower it for a body with high thermal inertia in some models of thermal emission). Many of the smaller TNOs have $A \approx 5\%$, while the largest TNOs have $A \approx$ 60-80% (Lellouch et al. 2013). Thus, the temperatures relevant for TNOs range from $T_{ss} \approx 70$ K for ϵ=1, η=1, A = 5% at R=30 AU down to $T_{avg} \approx 20$ K for $\epsilon = 1$, $\eta = 1$, A = 80% at 90 AU. Detached objects at R much greater 90 AU will have even colder temperatures. Eq (1) ignores latent heat of sublimation, the conduction of heat into for from the subsurface (see Section 4), and internal heat flux.

The surface pressure of an atmosphere over a pure ice in thermodynamic equilibrium (the sublimation pressure, $p_s(T_0)$) is a function only of the ice temperature (Fray & Schmitt 2009). Of the three super-volatiles seen in the outer solar system, N_2, CO, and CH_4, N_2 is by far the most volatile (Fig 1). TNOs with volatiles show a mix of ices: CH_4 or CO diluted in N_2-rich ice; N_2 or CO diluted in CH_4-rich ice; or pure CH_4 ices. The mixtures present complicated surface-ice interaction, including lag deposits and the influence of CH_4-rich warm patches (see review by Trafton et al. 1998). Trafton (2015) and Tan and Kargel (2018) have more recent work on the mixtures, including in particular the three-phase equilibrium between CH_4 saturated in N_2-rich ice, N_2 saturated in CH_4 ice, and N_2-CH_4 gas, but these have not tested under laboratory conditions. Moreover, as seen in the Fray and Schmitt (2009) compilation, laboratory measurements for the pure ices only exist for temperatures above 54.78 K for CO and above 48.15 K for CH_4; and the only laboratory data below 35.4 K for N_2 were published in 1960 (Borovik et al. 1960).

INSERT FIG 1 HERE

The surface pressure is approximately the weight of the column of gas, and so is closely related to the column density at the surface, N_0

(2) $$p_s(T_0) \approx mg_0N_0 \approx mg_0H_0n_0$$

where m is the mass of molecule, and g_0 is surface gravity, given by $g_0 = GM/r_0^2$, where G is the gravitational constant, $M = \rho(4/3)\pi r_0^3$ is the TNO mass, ρ is the TNO bulk density, and r_0 is the surface radius. $H_0 = kT_0/mg_0$ is the pressure scale height at the surface, k is Boltzman's constant, and n_0 is the local number density at the surface.

For small column densities, the atmosphere can be described as a surface-bounded exobase, since if $N_0\ \sigma_{eff} << 1$, where σ_{eff} is the effective collision cross section, then an escaping molecule is not likely to suffer a collision on its way out. This condition is equivalent to a large Knudsen number, Kn, the ratio of the mean free path between collisions, $l_{mfp} = 1/(n_0\ \sigma_{eff})$, to the a characteristic length scale. The scale in question depends on the problem at hand; taking the scale height for the length scale (Zhu et al. 2014), $Kn = 1$ is one classic definition of an exobase. At the surface:

(3) $$Kn_0 = \frac{l_{mfp}}{H_0} = \frac{1}{N_0\sigma_{eff}}$$

Since $\sigma_{coll} \approx 0.46x10^{-14}$ for CH_4 (Atkins and de Paula 2009) or $\sigma_{coll} \approx 0.43x10^{-14}$ for N_2 (Kaye and Laby 1973), with some dependence on temperature, bodies with N_0 greater than ~ 1.6 x 10^{14} molecule cm^{-2} can be considered collisional. This is achieved for N_2 or CH_4 at extremely small surface pressures (Fig 1), ~10^{-8} to 10^{-6} μbar for radii of 100 to 1000 km. Extrapolating to these small pressures from the pressures measured in the lab is questionable, but application of the Fray and Schmidt compilations predicts that the transition to continuum atmospheres happens near temperatures of ~29 K for CH_4, and ~21 K for N_2, depending weakly on the TNO radius and density. For larger column densities, the atmosphere opaque to UV radiation. This transition occurs at N_0 ~10^{18} molecule cm^{-2} (T_0 ~ 26 K) for N_2 with 3% CH_4 gaseous molar mixing ratio, or N_0 ~3x10^{16} molecule cm^{-2} (T_0 ~ 32 K) for pure CH_4 (Johnson et al. 2015).

The Jeans parameter at the surface, or ratio of potential energy to thermal energy, is a measure of how tightly bound the atmosphere is, and is given by:

(4) $$\lambda = \frac{gm}{rkT} = \frac{U}{kT} = \frac{r}{H} = \frac{GMm}{r^2}$$

The Jeans parameter at the surface, λ_0, varies from ~0.1 (unbound) for CH_4 gas on 100-km radius objects at 70 K to ~100 (bound) for N_2 gas on 1000-km radius objects at 20 K. Although the composition surely varies from object to object, assuming each TNO has N_2 on its surface it can be seen from Fig. 2 that due to the large range of temperatures, the TNO atmospheres can have a large range of λ_0 and N_0, which, of course, makes these objects interesting, with implications for atmospheric escape, seasonal variation, and detectability.

INSERT FIG 2 HERE

3. Expected volatile retention

In general, only the largest TNOs have had volatiles detected or suspected on their surfaces (Table 1). This is not merely an observational effect (i.e., because higher quality spectra are more easily obtained on larger TNOs), but is linked to the escape of their initial inventory of volatiles (Schaller & Brown 2007a; Johnson et al. 2015). Volatile escape can be driven by heating of the surface by solar visible radiation, and by absorption of solar radiation in the atmosphere. The relative importance of these processes depends on how tightly bound the atmosphere is, parameterized by the surface Jean's parameter λ_0, and its UV opacity, parameterized by its surface column density, N_0. Since the work of Schaller & Brown (2007a), there has been progress in the escape rate in the transition to the fluid regime for transparent atmospheres (Volkov et al. 2011a,b), the role of atmospheric heating on escape (Johnson et al 2013a,b, 2015), as well as new observations relating to the initial inventories (Glein & Waite 2018) and the complexity of escape at Pluto (Gladstone & Young 2019).

In order to provide a link between the presence of volatiles, the bulk properties, and the orbits of TNOs, Schaller & Brown (2007a) considered sublimation-induced escape directly from the TNOs surface. Starting with the equilibrium surface temperature (e.g., Eq. 1 with $\bar{\mu} = 1/4$ and $\eta = 1$), they used the Jeans expression for escape from an exobase, evaluated at the conditions of the surface (subscripted here as *SJ* for surface-Jeans):

(5) $$\Phi_{SJ} = 4\pi r_0^2 n_0 (\bar{v}/4)(1 + \lambda_0)\exp(-\lambda_0)$$

where Φ is the total escape rate of volatiles in molecule s^{-1}, and $\bar{v} = \sqrt{8kT/\pi m}$ is the mean molecular speed. Using these expression for T_0 and Φ, they divided the TNOs into those that would likely keep their volatiles and those that likely lost their initial volatile inventory over the age of the solar system (Fig 3).

INSERT FIG 3 HERE

The surface-Jeans estimate of the escape rate is roughly accurate if the atmosphere is non-collisional, $N_0 < \sim 10^{14}$ molecule cm^{-2} (Fig 4), which holds for very distant TNOs. However, Eq. 5 is problematic, even for atmospheres that are transparent to solar heating. Volkov et al. (2011a, b) used a molecular kinetic model, the Direct Simulation Monte Carlo (DSMC) method (Bird 1994), to calculate the surface-heated escape rate, Φ_S, from a single-component atmosphere for a range of surface values of T_0 and N_0, and then expanded this range to very thick atmospheres using a fluid model. Note that Volkov et al. (2011a, b) use the *radial* Knudsen number, scaling the mean-free-path by the surface radius, denoted here as Kn_0^r (*r* for radial). This is related to Eq (3) through $Kn_0^r = l_{mfp}/r_0 = Kn_0 / \lambda_0$. Johnson et al. (2015) fit an analytic expression to the numerical results of Volkov et al. (2011a, b) to find a correction factor that depends on the surface values of the Knudsen number and Jean parameter:

(6) $$\Phi_S = \Phi_{SJ}/[(Kn_0^r)^{0.09} + \lambda_0^{2.55}\exp(-\lambda_0)/(70Kn_0^r)]$$

For cold atmospheres or large bodies (high gravity), the Jeans escape rate driven only by the surface temperature is throttled for a bound atmosphere by the exp(-λ) term (Fig 4). This can be overcome by direct absorption of solar radiation in the atmosphere. Assuming ~2-3% CH_4 in the more volatile N_2 background gas, Johnson et al. (2015) calculated that a column of gas is sufficient that the UV and EUV are primarily absorbed in the atmosphere for $N_0 > N_C$, where $N_C \approx 10^{18}$ molecule cm^{-2} is the minimum column for UV absorption. Prior to the New Horizon encounter, models of Pluto's atmospheric loss coupled a fluid simulation to a DSMC molecular kinetic simulation (e.g., Erwin et al. 2013; Tucker et al. 2012) to describe the absorption at depth as well as the escape from the exobase region. In their models, the simulated loss rate was matched reasonably well by the simple so-called energy limited escape model, in which the gravitational energy lost by the escaping molecules is set by the absorbed UV radiation. The applicability of that model was subsequently explored further (Johnson et al. 2015) and applied to other KBOs. Lyα dominates the absorbed UV flux if CH_4 is optically thick. Since scattered interplanetary Lyα and stellar flux contribute to the UV flux in the trans-Neptunian region, the energy-limited flux falls off more slowly than R^2. Eq. (7) gives the expression adopted by Johnson et al. (2015) for the escape due to heating in the upper atmosphere, Φ_U.

(7) $$\Phi_U = \Phi_P(\rho_P/\rho)[(30/R)^2 + 0.09]$$

where ρ_P and ρ are is the density of Pluto and the TNO, R is the heliocentric distance in AU, and Φ_P is the escape rate at Pluto. Johnson et al. (2015), based on Erwin et al. 2013 and Tucker et al. 2012, adopted $\rho_P = 2.05$ g cm^{-3}, and $\Phi_P = 120$ kg s^{-1} / $m_{N2} = 2.6\times10^{27}$ N_2 s^{-1}. Johnson et al. (2015) combined surface and upper atmospheric heating by restricting Φ_U to $N_0 > N_C$ and choosing the larger of Φ_S and Φ_U (Fig 4). Fig. 4 only gives a rough guide for ranges in which global models of the two escape processes dominate. Johnson et al. (2015) used the combined atmospheric loss rates over the lifetime of individual TNOs (Table 2 in Johnson et al. 2015, which did not include Orcus and Varuna). Besides Charon, which has likely lost its initial volatiles, they concluded that for the objects studied only Makemake, Quaoar and 2007 OR10 likely lost a large fraction of their volatiles, primarily due to short wavelength absorption in their upper atmospheres.

INSERT FIG. 4 HERE

This picture has been altered by two recent spacecraft measurements. One is our more recent understanding of Pluto's atmosphere based on the New Horizons observations (Gladstone and Young 2019). Prior to the flyby, the expected escape rate was ~[0.4-4] x 10^{27} N_2 s^{-1} (Zhu et al. 2014), consistent with energy-limited escape. The derived escape from the observed profile is much lower: (3–7) × 10^{22} N_2 s^{-1} and (4–8) × 10^{25} CH_4 s^{-1} (Young et al 2018). Applying our new insight has been confounded by the fact that the principal cooling agent in Pluto's upper atmosphere is still uncertain (Gladstone & Young 2019). The second is new constraints on the initial inventory of volatiles. While Schaller & Brown 2007a and Johnson et al. 2015 used an N_2 to H_2O mass ratio of 2%, Glein & Waite (2018) use the mixing ratio of N_2 measured in the coma of 67P (Rubin et al., 2015) to derive an N_2 to H_2O mass ratio of only [0.7-6]x10^{-4}.

In summary, the inclusion of escape from energy deposited in the upper atmosphere can move the retention lines to the right, especially for N_2 above ~25 K. The New Horizons results may temper the increase due to atmospheric heating. The new data on a smaller original N_2

inventory would also move retention lines to the right. It is clear from the simulation results described here that the connection between the surface properties and atmospheric escape is subtle, but it also is likely more interesting than initially suggested.

4. Variation of atmospheres over an orbit

Because the sublimation pressures depend exponentially on the temperatures of the volatile ices, the gases surrounding volatile-bearing TNOs vary with heliocentric distance and subsolar latitude, and possibly time of day. This was initially modeled for Triton and Pluto (see reviews by Spencer et al. 1997 and Yelle et al. 1995). Since those reviews, a trend of increasing atmospheric pressure for both Triton and Pluto were observed using the technique of stellar occultation, with an increase by factors of two and three respectively (Elliot et al. 1998; Olkin et al. 2015). The new time-base of atmospheric observations and the New Horizons flyby of Pluto inspired new models of seasonal variation (e.g., Young 2012, 2013, 2017; Hansen et al. 2015; Olkin et al. 1997, 2015), including general circulation models (e.g., Forget et al. 2017) and evolution of atmospheres on the timescale of millions of years (e.g., Bertrand et al. 2016, 2018).

When N_2 was discovered on the surface of Eris, authors speculated that volatiles on TNOs, especially N_2, could raise temporary atmospheres near perihelion (e.g., Dumas et al. 2007). This was generalized in Stern and Trafton (2008), and applied numerically to the known or suspected volatile-bearing TNOs by Young & McKinnon (2013). When thinking about atmospheres on TNOs, it is useful to distinguish three types: global, collisional, and ballistic. For global sublimation-supported atmospheres, such as Mars or current-day Pluto and Triton, volatiles sublime from areas of higher insolation, and recondense on areas of lower insolation, transporting latent heat as well as mass (Trafton 1984, also see reviews by Spencer et al. 1997; Yelle et al. 1995; Stern and Trafton 2008). As long as the volatiles can be effectively transported, the surface pressures and the volatile ice temperatures will be nearly constant across the surface. Sublimation winds transport mass from latitudes of high insolation to low insolation. Trafton (1984) showed that pressures stay within 10% across the surface if the sublimation winds (v) are less than 7.2% of the sound speed (v_s). The sublimation wind speeds can by found by conservation of mass: the mass per time crossing a given latitude equals the integral of the net deposition from that latitude to the pole. The wind speeds depend on the subsolar latitude (Trafton 1984), if we consider diurnally averaged insolation; higher wind speeds are needed to transport volatiles pole-to-pole (high subsolar latitudes) than equator-to-pole (low subsolar latitudes). For an "ice ball" uniformly covered in volatiles, the maximum sublimation wind speed, v, can be expressed as

(8) $$vmN_0 = \xi Sr/L$$

where $S = S_{1AU}(1-A)/R^2 = 4\varepsilon\sigma T_{avg}^4$ is the absorbed normal insolation, and L is the latent heat of sublimation, in energy per mass. ξ in Eq. 8 is a numerical factor accounting for the subsolar latitude, λ_{sun}. We calculated ξ numerically, following the prescription of Young (1992). From these calculations, ξ is well approximated by a cubic expression

(9) $$\xi(\lambda_{sun}) \approx 0.044 + 0.148\,(\lambda_{sun}/90°) + 0.4012\,(\lambda_{sun}/90°)^2 - 0.296\,(\lambda_{sun}/90°)^3$$

For a 400-1400 km radius body uniformly covered with CH_4 ice to have a global atmosphere, the pressure needs to be greater than ~10 to 290 nbar for polar illumination (3.4×10^{19} to 1.8×10^{20}

cm^{-2}, 40.3 to 45.5 K; Fig 5), or 0.8 to 22 nbar for equatorial ($2.6 x 10^{18}$ to $1.3 x 10^{19}$ cm^{-2}, 37.1 to 41.4 K). For N_2, the pressures are similar, so the temperatures are lower: 12 to 262 nbar for polar ($1.8 x 10^{19}$ to $9.1 x 10^{19}$ cm^{-2}, 28.8 to 32.1 K) or 1 to 20 nbar for equatorial ($1.4 x 10^{18}$ to $6.8 x 10^{18}$ cm^{-2}, 26.6 to 29.3 K) for N_2. As observations of Pluto, Triton and Mars demonstrate, global atmospheres show a variety of phenomena, such as boundary layers, waves, atmospheric chemistry, and haze formation.

The temperatures in Fig 5 are highly simplified. Thermal inertia can be important, even at the long timescales in the outer solar system. More significantly, bodies are unlikely to be uniformly covered in volatiles. For example, much of the N_2 on Pluto is located in the basin known as Sputnik Planitia (Moore et al. 2016), and Triton's N_2 may be perennially confined to the South pole (Moore & Spencer 1990).

INSERT FIG. 5 HERE

Non-global atmospheres will vary with location and time-of-day, but may still be collisional, if the column density is greater than ~10^{14} cm^{-2} for either N_2 or CH_4. Io is a classic example of a local atmosphere that is collisional around the sub-solar point, and demonstrates some of the processes in even these thin atmospheres. Atmospheric chemistry can occur even in these tenuous atmospheres (Wong & Smyth 2000). Supersonic winds certainly flow and transport volatiles, even if they are not effective at equalizing pressures and temperatures (e.g., Walker et al. 2012). Recently, Hofgartner et al. (2018) used the Ingersoll et al. (1985) meteorological model developed for Io study the transport of N_2 on Eris at aphelion, when it is a local, collisional atmosphere, and found significant transport of N_2 ice. Even for more tenuous "surface-bounded exospheres," the loss of volatiles can modify landforms (see review by Mangold 2011). For example, sublimation erosion may lead to the narrow divides between craters on Hyperion (Howard et al. 2012) or redeposition on the crater rims on Callisto, where the convex summits see less of the warm surface than do concave crater interiors, and are therefore local cold traps (Howard and Moore 2008).

5. Detections of or limits on atmospheres by stellar occultation.

While other techniques can constrain the surface composition, thermal properties, rotation, and mass of distant TNOs, the technique of stellar occultation is by far the most powerful way to search for atmospheres around these bodies, as well as to study their size, shape, and the presence or nature of rings or jets (see Ortiz et al., this volume; Elliot and Olkin 1996, Elliot & Kern 2003; Santos-Sanz et al 2016). In an occultation, the starlight is refracted through a bending angle that increases in magnitude roughly in proportion to the line-of-sight column density (N_{los}). This leads to differential refraction, or a divergence of the refracted rays (cf Elliot and Olkin 1996), which dims the occulted starlight according to the scale height H and the column density. Some insight can be gained (Fig. 6) from the approximate, analytic expression for the relative stellar flux (e.g., Elliot and Young 1992):

(10) $$\phi \approx \left(1-\theta\frac{\Delta}{H}\right)^{-1}\left(1+\theta\frac{\Delta}{r}\right)^{-1} e^{-\sigma_{ext}N_{los}}$$

where θ is the bending angle, given by $\theta \approx -\nu_{STP} N_{los}/n_{STP} H$, ν_{STP} is the refractivity at standard temperature and pressure (2.9x10^{-4} and 4.4x10^{-4} for N_2 and CH_4 at 0.7 μm), n_{STP} is Loschmidt's constant (2.6868x10^{19} cm^{-3}), and Δ is the target-observer distance. As before, r is the radius (distance from target center) and H is the atmospheric scale height. N_{los} is the line-of-sight column density (molecule per area), which is larger than N, the vertical column density, by the unitless factor $\sqrt{2\pi\lambda}$ (e.g. 8-25 for $\lambda \approx$10-100). σ_{ext} is the extinction cross section (area per molecule). The first term represents the decrease due to the divergence (defocusing) of rays perpendicular to the limb, and halves the starlight when $\theta\Delta \approx -H$. The second term represents the increase due to refocusing parallel to the limb, leading to a "central flash" near the center of the body; the considerations of wave optics avoids division by zero at the shadow center when $\theta\Delta \approx -r$. The final term represents extinction, which becomes important when $N_{los} \approx 1/\sigma_{ext}$ (e.g., $N_{los} \approx 10^{26}$ molecule cm^{-2} for Rayleigh scattering at visible wavelengths, or $N_{los} \approx 10^{17}$ molecule cm^{-2} for typical crosssections in the extreme ultraviolet (UV)). Refraction is typically dominant over extinction for Earth-based stellar occultations of TNOs, and extinction dominates for spacecraft UV occultations.

INSERT FIG. 6 HERE

Lightcurves from model atmospheres can be calculated analytically for some idealized atmospheres (Elliot and Young 1992). However, the presence of CH_4 or its by-products (including photochemical haze) can heat up the atmosphere by 10s of K (Yelle and Lunine 1989, Zhang et al. 2018). For more complex atmospheres, synthetic lightcurves are calculated under the assumption of geometric optics/ray-tracing (Sicardy et al. 1999 and references therein) or wave optics/Fresnel diffraction (French and Gierasch 1976). Standard model fitting can then be used to extract the geometric edge and the refractivity of the atmosphere at the surface. For high quality data (as has been obtained for Pluto and Triton), lightcurves can be inverted to extract temperature, pressure, and number-density profiles (e.g. Elliot et al. 2003b). Derived surface pressures (or upper limits) from occultation lightcurves can be compared to the sublimation pressures for the atmospheric molecules under consideration, as expected from its surface equilibrium temperature (Fray and Schmitt 2009).

Synthetic light curves vs. shadow radius are plotted in Fig 7 for an example TNO with an N_2 or CH_4-dominated atmosphere (see caption for model details). Typical sky-plane velocities are 20 km s^{-1}, dominated by the Earth motion, and very slow events can improve detectability or limits. Very thin atmospheres (10's to 100's of nanobar, or ~10^{19} to 10^{20} molecule cm^{-2}) will only promote a small drop of flux very close to the surface, so very high signal to noise ratio is required for detection. Denser atmospheres (a few μbar, or ~10^{20} molecule cm^{-2}) cause a gradual drop in the star flux at a significant distance from the object's surface, so they will be easier to detect. For denser atmospheres, the ray that grazes the TNO surface is refracted inward significantly towards smaller shadow radii (bent by 94 to 112 km for 1 μbar CH_4 or N_2 atmospheres). For the 10 microbar curve, the surface-grazing ray is refracted past the shadow center. The bottom flux never reaches zero and much of the lightcurve is the sum of the near and far limb contributions. In the example plotted, the limb-grazing ray is bent by 900 to 1180 km for a CH_4 or N_2 atmospheres, leading to the discontinuities seen at ±400 km or ±680 km for the CH_4-or the N_2-dominated atmospheres. When the star crosses the center of the object as seen from Earth, it causes a prominent central flash for the 10 microbar atmosphere, as the atmosphere acts as a lens, converging the starlight from all parts of the atmosphere to the observer.

INSERT FIG 7 HERE

Stellar occultations by Pluto, Charon, and Triton, have been observed since the 1980's. *Pluto*: A single-chord occultation from 1985 observed under extremely difficult circumstances was reported in 1985 (Brosch 1995). The definitive discovery of Pluto's atmosphere was from the 1988 stellar occultation (Hubbard et al. 1988, Millis et al. 1993). Observations in 2002 showed a doubling of the pressure (Sicardy et al 2003; Elliot et al. 2003a). Many high-quality observations since have revealed the changes in Pluto's atmosphere, its thermal structure, and waves (Young et al. 2008; Sicardy et al. 2016; Pasachoff et al. 2017). *Triton*: Triton, like Pluto, has had several high-quality occultations, and has also shown large changes in the surface pressure on decadal timescales (Elliot et al. 1998; Elliot et al. 2000). *Charon*: Prior to the New Horizons flyby, limits on Charon's atmosphere were set to be < 50 nbar (1-σ) from stellar occultation (Gulbis et al. 2006), and the New Horizons UV occultation set limits of < 1.4 pbar (Stern et al. 2017).

Since 2009, stellar occultations have been successfully used to study other TNOs, and the search for an atmospheric signature was carried for a few of them. Most of the largest bodies have already observed during a stellar occultation event and no atmosphere around a TNO has been found so far (other than Pluto and ex-TNO Triton). Upper limits on the presence of putative atmospheres were obtained and they are summarized below and in Table 2.

Eris: A stellar occultation of a V = 17.1 star by Eris was observed on November 06, 2010 (Sicardy et al. 2011). Eris, the second biggest TNO after Pluto, was at 95.7 AU and had a near surface temperature estimated at 30 K. With methane and nitrogen detected on its surface, it was a good candidate to have retained an atmosphere. The occultation allowed a constraint on the presence of an isothermal N_2 atmosphere to an upper limit of 1 nbar at the surface, with similar limits for CH_4 and argon. The occultation revealed that Eris is one of the brightest objects of the solar system, with a geometrical albedo of p_v= 0.96 (+0.09/-0.04), which may be caused by a collapsed atmosphere, as discussed above. As the sub-solar temperature of Eris can reach 32 K, the authors mentioned that a local sub-solar atmosphere of N_2 may exist, but it would freeze to undetectable values at the limb. It is suggested that, due to the eccentric orbit of Eris, when it approaches its perihelion at 37.8 AU, it may develop a global atmosphere of 2 μbar (see section 3).

Haumea: The third biggest TNO, the largest member of the only known collisional family of the transneptunian region, with two big moons, a rotation of 3.9 hours, elongated shape and possibly a localized dark spot on its surface, Haumea was already one of the most interesting TNOs. An observation of a stellar occultation on the 21st February 2017 revealed that it also possesses a dense ring of 70 km in width (Ortiz et al., 2017), making it as the second small solar system object, after (10199) Chariklo (Braga-Ribas et al., 2014a), known to have a ring. Although no evidence of CH_4 or N_2 is present on spectroscopic observations of its surface, the occultation data was searched for signatures of a putative atmosphere. Considering the distance of 50.6 AU and its geometric albedo of 0.51, its surface temperature was modeled to be 40 K. For a CH_4 atmosphere a 1 σ upper limit of P_{surf} < 10 nanobar was obtained, limited by the quality of the data. For an isothermal N_2 atmosphere, an upper limit of P_{surf} < 3 nbar (1-σ level) was derived.

Makemake: One of the five biggest TNOS, Makemake, occulted a V = 18.5 star on April 23, 2011 (Ortiz et al., 2012). The event was detected from seven telescopes in Chile (including VLT and NTT), allowing the measurement of its size, shape, and study of its close vicinity. With a geometric albedo of 0.77, a surface temperature of about 50 K, as inferred from Herschel Space Observatory observations, and CH_4 ice detected on its surface (although N_2 seem to be almost absent), it was a candidate to possess a global atmosphere (see section 2). The observation revealed no global atmosphere around Makemake. Ortiz et al., (2012) modeled a pure CH_4 atmosphere, starting with a temperature of 30 K heated by the near-IR radiation from the methane bands up to 100 K reaching an isothermal branch. The comparison of the model with the data from NTT gives an upper limit of 8 nbar for the surface pressure (P_{surf}) at 1 sigma level. With a 40 K surface temperature, the upper limit increases to P_{surf} < 11 nbar for the surface pressure. Considering a more relaxed limit of 3 σ, the upper limit for the surface pressure reaches 100 nbar. If the atmosphere is made of a mixture of N_2 and CH_4 it would have a similar temperature profile, and the upper limit P_{surf} < 12 nbar, and a pure N_2 isothermal atmosphere P_{surf} < 4 nbar. So all the tested models are compatible with a no detection of a global atmosphere with upper limits for the surface temperature from 4 to 12 nbar at 1-σ level. The conclusion is that Makemake has lost almost all of its N_2 gas or, a possible explanation, is in a pole-on orientation that would freeze the atmosphere near the limb to undetectable values. Some points close to centrality have an elevated flux, a few σ above the noise, which have raised the discussion of local atmospheres. Since the sub-solar temperature for Makemake would be on the order of 50-55 K at a distance of 51.5 AU and geometric albedo 0.77, a local patch of methane could produce an atmosphere of P_{surf} = 3-25 μbar. With the rotation of the object, this can lead to a band of localized atmosphere. Playing with the size and orientation of this band of atmosphere, the synthetic light curves could fit to the observations. An N_2 localized atmosphere of P_{surf} = 30 μbar, for a surface temperature of 38 K produced a central flash too large for the data, but an N_2 atmosphere with P_{surf} <10 μbar would cause bumps small enough to be hidden in the noise level. The conclusion is that localized atmosphere of CH_4 or N_2 are not ruled out by the data, but there are too many unknown parameters to safely affirm that Makemake has a localized atmosphere.

Quaoar: a large TNO with (r_0 = 550 km) and CH_4 reported on its surface, Quaoar was a candidate to possess a thin atmosphere. It was observed crossing in front of a star on May 4, 2011, from which upper limits on the presence of an atmosphere were derived (Braga-Ribas et al., 2013). Being at a distance of 42.4 AU, with a geometric albedo of 0.109, a surface equilibrium temperature of 40 K is expected. Considering a CH_4 dominant atmosphere, reaching 102 K above 10 km from the surface, an upper limit of P_{surf} < 21 nbar (1-σ) was obtained. As N_2 would have a vapor pressure of 176 microbar at the same temperature, the data rule out this scenario.

INSERT TABLE 2 HERE

Smaller TNOS: Additional TNOs have been observed during stellar occultations, and no clear signals of any atmosphere were detected. For these, the decrease in stellar flux was abrupt (rather than dimming by atmospheric refraction), or the data did not have high enough quality (cadence or signal-to-noise ratio) for any speculation about the presence or absence of an atmosphere. The larger bodies (equivalent radii r_0 > 200 km) so probed include: Varuna (r_0 = 568 km; Sicardy et al. 2010), 2003 VS_2 (r_0 = 561 km; Rossi et al. 2017), 2002 TC_{302} (r_0 = 499 km; Santos-Sanz et al. 2017), 2003 AZ_{84} (r_0 = 382 km; Dias-Oliveira et al. 2017) and 2007 UK_{126} (319 km; Benedetti-Rossi et al. 2016).

6. Future research

The above discussion suggests some critical directions for future research.

Surface Compositions:

- The changing compositions of Triton (visual magnitude *V*=13.4) and Pluto (*V*=14.2) can and should continue to be tracked with moderate ground-based telescopes.
- For other large TNOs, new understanding the surface stratification of CH_4 and N_2 on Eris (*V*=18.7) needs higher spectral resolution and SNR than previous spectra, as does the confirmation of, or constraints on, CH_4 on Quaoar (V=18.7), 2007 OR_{10} (V=21.3), Sedna (*V*=20.8), Varuna (*V*=20.1), and Orcus (*V*=19.2). Some progress is likely to come from the new generation of infrared detectors (e.g., NIRES on Keck, or NIHTS on DCT). JWST's spectral sensitivity from 1-5 microns will be very powerful for measuring the volatiles and other species on the surfaces of these and other TNOs (Parker et al. 2016). Both the Thirty Meter Telescope and the European Extremely Large Telescope have planned near-infrared integral field spectrometers as first light instruments, and their various white papers emphasize how they will revolutionize TNO spectroscopy.

Laboratory work:

- The vapor pressures of CO and CH_4 should be measured at TNO temperatures of 20-40 K, and the vapor pressures of N_2 should be remeasured in a modern lab. Recent work on the vapor pressures of mixed volatile ices should be also tested under laboratory conditions.
- Measurements of the spectrum of CH_4 ice in the visible, both pure and in solution with N_2, is needed for quantitative analysis of Makemake's CH_4 features 0.54-0.62 μm.

Atmospheric retention and escape:

- The most critical work is a better model of why the escape rate at Pluto in 2015 is so much lower than the expected energy-limited rate, and how that model can be applied to Pluto at other seasons, and to other TNOs.
- The N_2/CH_4 mixed surfaces suggest new DSMC work with multiple species. Similarly, local atmospheres (e.g., dome-like atmospheres over the subsolar point) can be more completely modeled.

Seasonal:

- Models such as Hofgartner et al. (2018) can be used to investigate the transition between global and collisional atmospheres.

Atmospheric searches:

- Accurate star positions are now given by Gaia catalogue, but ephemeris errors are nearly always much greater than the object's apparent angular size. Astrometric positions are needed. One source of positions can be the big and deep surveys like the Large Synoptic Sky Survey that is currently under construction and will start the observations in 2022, and will help to update the TNOs ephemeris and so to have accurate stellar occultation predictions (Camargo et al. 2018).

Acknowledgments

Leslie Young was supported in part by the NASA OPR grant NNX14AO45G "Connecting Present and Past KBOs." Felipe Braga Ribas acknowledges CNPq grant 309578/2017-5.

References

Abernathy, M. R., S. C. Tegler, W. M. Grundy, J. Licandro, W. Romanishin, D. Cornelison, et al. 2009. Digging into the surface of the icy dwarf planet Eris. Icarus 199, 520-525.

Armstrong, G.T., Brickwedde, F.G., Scott, R.B., 1955. Vapor pressures of methanes. J. Res. Natl. Bur. Stand. 55 (1), 39–52.

Atkins, P. and J. de Paula 2009. Elements of Physical Chemistry 5th ed, Oxford University Press.

Barucci, M. A. and F. Merlin 2019. Surface composition of Transneptunian Objects. This volume.

Barucci, M. A., D. P. Cruikshank, E. Dotto, F. Merlin, F. Poulet, C. Dalle Ore, et al. 2005. Is Sedna another Triton? Astronomy and Astrophysics 439, L1-L4.

Barucci, M. A., F. Merlin, A. Guilbert, C. de Bergh, A. Alvarez-Candal, O. Hainaut, et al. 2008. Surface composition and temperature of the TNO Orcus. Astronomy and Astrophysics 479, L13-L16.

Barucci, M. A., C. Morea Dalle Ore, A. Alvarez-Candal, C. de Bergh, F. Merlin, C. Dumas et al. 2010. (90377) Sedna: Investigation of surface compositional variation. The Astronomical Journal 140, 2095-2100.

Barucci, M. A., C. M. Dalle Ore, D. Perna, D. P. Cruikshank, A. Doressoundiram, A. Alvarez-Candal et al. 2015. (50000) Quaoar: Surface composition variability. Astronomy and Astrophysics 584, A107.

Benedetti-Rossi, G., and 28 colleagues 2016. Results from the 2014 November 15th Multi-chord Stellar Occultation by the TNO (229762) 2007 UK_{126}. The Astronomical Journal 152, 156.

Bertrand, T. and F. Forget 2016. Observed glacier and volatile distribution on Pluto from atmosphere-topography processes. Nature 540, 86-89.

Bertrand, T. and F. Forget 2017. 3D modeling of organic haze in Pluto's atmosphere. Icarus 287, 72-86.

Bertrand, T., and 14 colleagues 2018. The nitrogen cycles on Pluto over seasonal and astronomical timescales. Icarus 309, 277-296.

Bird, G. A. 1994, Molecular Gas Dynamics and the Direct Simulation of Gas Flows (Oxford: Clarendon).

Borovik, E.S., Grishin, S.F., Grishina, E.Y., 1960. The vapor pressure of nitrogen and hydrogen at low pressures. Sov. Phys. Tech. Phys. (Engl. Transl.) 5 (5), 506–511.

Braga-Ribas, F., Sicardy, B., Ortiz, J. L. et al. 2013. The size, shape, albedo, density, and atmospheric Limit of Transneptunian Object (50000) Quaoar from multi-chord stellar occultations. Astrophysical Journal 773, 26.

Braga-Ribas, F., Sicardy, B., Ortiz, J. L. et al. 2014a. A ring system detected around the Centaur (10199) Chariklo. Nature 508, 72-75.

Braga-Ribas, F., R. Vieira-Martins, M. Assafin, J. I. B. Camargo, B. Sicardy, and J. L. Ortiz 2014b. Stellar Occultations by Transneptunian and Centaurs Objects: results from more than 10 observed events. Revista Mexicana de Astronomia y Astrofisica Conference Series 44, 3-3.

Broadfoot, A. L., and 21 colleagues 1989. Ultraviolet spectrometer observations of Neptune and Triton. Science 246, 1459-1466.

Brosch, N. 1995. The 1985 stellar occultation by Pluto. Monthly Notices of the Royal Astronomical Society 276, 571-578.

Brown, M. E., C. A. Trujillo, and D. L. Rabinowitz 2005. Discovery of a Planetary-sized Object in the Scattered Kuiper Belt. The Astrophysical Journal 635, L97-L100.

Brown, M. E., K. M. Barkume, G. A. Blake, E. L. Schaller, D. L. Rabinowitz, H. G. Roe et al. 2007. Methane and Ethane on the bright Kuiper Belt Object 2005 FY_9. The Astronomical Journal 133, 284-289.

Brown, M. E. 2008. The Largest Kuiper Belt Objects. The Solar System Beyond Neptune 335-344.

Brown, M. E., A. J. Burgasser and W. C. Fraser 2011. The surface composition of large Kuiper Belt Object 2007 OR_{10}. The Astrophysical Journal 738, L26.

Brown, M. E. 2012. The compositions of Kuiper Belt Objects. Annual Review of Earth and Planetary Sciences 40, 467-494.

Camargo, J. I. B., J. Desmars, F. Braga-Ribas, R. Vieira-Martins, M. Assafin, B. Sicardy et al. 2018. The future of stellar occultations by distant solar system bodies: Perspectives from the Gaia astrometry and the deep sky surveys. Planetary and Space Science 154, 59-62.

Carry, B., and 10 colleagues 2011. Integral-field spectroscopy of (90482) Orcus-Vanth. Astronomy and Astrophysics 534, A115.

Clayton, J.O., Giauque, W.F., 1932. The heat capacity and entropy of carbon monoxide. Heat of vaporization. Vapor pressures of solid and liquid. Free energy to 5000 K from spectroscopic data. J. Am. Chem. Soc. 54 (7), 2610–2626.

Cruikshank, D. P., T. L. Roush, T. C. Owen, T. R. Geballe, C. de Bergh, B. Schmitt et al. 1993. Ices on the surface of Triton. Science 261, 742-745.

Cruikshank, D. P., and 10 colleagues 2000. Water Ice on Triton. Icarus 147, 309-316.

Cruikshank, and 12 colleagues 2015.The surface compositions of Pluto and Charon. Icarus 246, 82-92.

Dalle Ore, C. M., and 12 colleagues 2009. Composition of KBO (50000) Quaoar. Astronomy and Astrophysics 501, 349-357.

Dalle Ore, C. M., M. A. Barucci, J. P. Emery, D. P. Cruikshank, C. de Bergh, T. L. Roush, D. Perna, F. Merlin and L. V. Dalle Ore 2015. The composition of "ultra-red" TNOs and centaurs. Icarus 252, 311-326.

de Bergh, C., A. Delsanti, G. P. Tozzi, E. Dotto, A. Doressoundiram and M. A. Barucci 2005. The surface of the Transneptunian Object 90482 Orcus. Astronomy and Astrophysics 437, 1115-1120.

de Bergh, C., E. L. Schaller, M. E. Brown, R. Brunetto, D. P. Cruikshank and B. Schmitt 2013. The Ices on Transneptunian Objects and Centaurs. Astrophysics and Space Science Library 356, 107.

Delsanti, A., F. Merlin, A. Guilbert-Lepoutre, J. Bauer, B. Yang, and K. J. Meech 2010. Methane, ammonia, and their irradiation products at the surface of an intermediate-size KBO? A portrait of Plutino (90482) Orcus. Astronomy and Astrophysics 520, A40.

DeMeo, F. E., M. A. Barucci, F. Merlin, A. Guilbert-Lepoutre, A. Alvarez-Candal, A. Delsanti, et al. 2010. A spectroscopic analysis of Jupiter-coupled object (52872) Okyrhoe, and TNOs (90482) Orcus and (73480) 2002 PN_{34}. Astronomy and Astrophysics 521, A35.

Dias-Oliveira, A., Sicardy, B., Ortiz, J. L. et al. 2017. Study of the Plutino Object (208996) 2003 AZ84 from Stellar Occultations: Size, Shape, and Topographic Features. The Astronomical Journal 154, 22.

Dumas, C., F. Merlin, M. A. Barucci, C. de Bergh, O. Hainault, A. Guilbert, P. Vernazza, and A. Doressoundiram 2007. Surface composition of the largest dwarf planet 136199 Eris (2003 UB_{313}). Astronomy and Astrophysics 471, 331-334.

Elliot, J. L. and L. A. Young 1992. Analysis of stellar occultation data for planetary atmospheres. I - Model fitting, with application to Pluto. The Astronomical Journal 103, 991-1015.

Elliot, J. L. and C. B. Olkin 1996. Probing planetary atmospheres with stellar occultations. Annual Review of Earth and Planetary Sciences 24, 89-124.

Elliot, J. L. and S. D. Kern 2003. Pluto's atmosphere and a targeted-occultation search for other bound KBO atmospheres. Earth Moon and Planets 92, 375-393.

Elliot, J. L., and 13 colleagues 1998. Global warming on Triton. Nature 393, 765-767.

Elliot, J. L., D. F. Strobel, X. Zhu, J. A. Stansberry, L. H. Wasserman, and O. G. Franz 2000. NOTE: The Thermal Structure of Triton's Middle Atmosphere. Icarus 143, 425-428.

Elliot, J. L., A. Ates, B. A. Babcock, A. S. Bosh, M. W. Buie, K. B. Clancy et al. 2003a. The recent expansion of Pluto's atmosphere. Nature 424, 165-168.

Elliot, J. L., M. J. Person, and S. Qu 2003b. Analysis of stellar occultation Data. II. Inversion, with application to Pluto and Triton. The Astronomical Journal 126, 1041-1079.

Emery, J. P., C. M. Dalle Ore, D. P. Cruikshank, Y. R. Fernández, D. E. Trilling and J. A. Stansberry 2007. Ices on (90377) Sedna: confirmation and compositional constraints. Astronomy and Astrophysics 466, 395-398.

Erwin, J., O. J. Tucker, and R. E. Johnson 2013. Hybrid fluid/kinetic modeling of Pluto’s escaping atmosphere. Icarus 226, 375-384.

Forget, F., T. Bertrand, M. Vangvichith, J. Leconte, E. Millour, and E. Lellouch 2017. A post-New Horizons global climate model of Pluto including the N_2, CH_4 and CO cycles. Icarus 287, 54-71.

Fornasier, S., E. Dotto, M. A. Barucci and C. Barbieri 2004. Water ice on the surface of the large TNO 2004 DW. Astronomy and Astrophysics 422, L43-L46.

Fray, N. and B. Schmitt 2009. Sublimation of ices of astrophysical interest: A bibliographic review. Planetary and Space Science 57, 2053-2080.

Frels, W., D. R. Smith, and T. Ashworth 1974. Vapour pressure of nitrogen below the triple point. Cryogenics 14, 3-7.

French, R. G. and P. J. Gierasch 1976. Diffraction calculation of occultation light curves in the presence of an isothermal atmosphere. The Astronomical Journal 81, 445-451.

Giauque, W.F., Clayton, J.O., 1933. The heat capacity and entropy of nitrogen. Heat of vaporization. Vapor pressures of solid and liquid. The reaction 1/2 N2+1/2 O2QNO from spectroscopic data. J. Am. Chem. Soc. 55 (12), 4875–4889.

Gladstone, G. R. and L. A. Young 2019. New Horizons observations of the atmosphere of Pluto. Annu. Rev. Earth Planet. Sci. 2019, in press.

Glein, C. R. and J. H. Waite 2018. Primordial N_2 provides a cosmochemical explanation for the existence of Sputnik Planitia, Pluto. Icarus 313, 79-92.

Grasset, O., J. Castillo-Rogez, T. Guillot, L. N. Fletcher, and F. Tosi 2017. Water and Volatiles in the Outer Solar System. Space Science Reviews 212, 835-875.

Grundy, W. M. and L. A. Young 2004. Near-infrared spectral monitoring of Triton with IRTF/SpeX I: establishing a baseline for rotational variability. Icarus 172, 455-465.

Grundy, W. M., L. A. Young, J. A. Stansberry, M. W. Buie, C. B. Olkin, and E. F. Young 2010. Near-infrared spectral monitoring of Triton with IRTF/SpeX II: Spatial distribution and evolution of ices. Icarus 205, 594-604.

Guilbert A. et al 2009. ESO-Large Program on TNOs: Near- infrared spectroscopy with SINFONI. Icarus 201, 272-283.

Gulbis, A. A. S., and 12 colleagues 2006. Charon's radius and atmospheric constraints from observations of a stellar occultation. Nature 439, 48-51.

Hansen, C. J., D. A. Paige, and L. A. Young 2015. Pluto's climate modeled with new observational constraints. Icarus 246, 183-191.

Hofgartner, J. D., B. J. Buratti, P. O. Hayne and L. A. Young 2018. Ongoing resurfacing of KBO Eris by volatile transport in local, collisional, sublimation atmosphere regime. Icarus, in press doi: https://doi.org/10.1016/j.icarus.2018.10.028.

Holler, B. J., L. A. Young, W. M. Grundy, and C. B. Olkin 2016. On the surface composition of Triton's southern latitudes. Icarus 267, 255-266.

Howard, A. D., J. M. Moore, P. M. Schenk, O. L. White, and J. Spencer 2012. Sublimation-driven erosion on Hyperion: Topographic analysis and landform simulation model tests. Icarus 220, 268-276.

Howard, A. D. and J. M. Moore 2008. Sublimation-driven erosion on Callisto: A landform simulation model test. Geophysical Research Letters 35, L03203.

Hubbard, W. B., D. M. Hunten, S. W. Dieters, K. M. Hill, and R. D. Watson 1988. Occultation evidence for an atmosphere on Pluto. Nature 336, 452-454.

Ingersoll, A. P., M. E. Summers, and S. G. Schlipf 1985. Supersonic meteorology of Io - Sublimation-driven flow of SO_2. Icarus 64, 375-390.

Jewitt, D. C. and J. Luu 2004. Crystalline water ice on the Kuiper belt object (50000) Quaoar. Nature 432, 731-733.

Johnson, R. E., A. Oza, L. A. Young, A. N. Volkov and C. Schmidt 2015. Volatile loss and classification of Kuiper Belt Objects. The Astrophysical Journal 809, 43.

Kaye, G. W. C. and Laby, T. H. 1973. Tables of physical and chemical constants, 14th ed. Longman Scientific & Technical, London.

Lellouch, E., and 16 colleagues 2013. "TNOs are Cool": A survey of the trans-Neptunian region. IX. Thermal properties of Kuiper belt objects and Centaurs from combined Herschel and Spitzer observations. Astronomy and Astrophysics 557, A60.

Licandro, J., N. Pinilla-Alonso, M. Pedani, E. Oliva, G. P. Tozzi, and W. M. Grundy 2006. The methane ice rich surface of large TNO 2005 FY_9: a Pluto-twin in the trans-neptunian belt?. Astronomy and Astrophysics 445, L35-L38.

Lorenzi, V., N. Pinilla-Alonso, J. Licandro, C. M. Dalle Ore, and J. P. Emery 2014. Rotationally resolved spectroscopy of (20000) Varuna in the near-infrared. Astronomy and Astrophysics 562, A85

Lorenzi, V., N. Pinilla-Alonso, and J. Licandro 2015. Rotationally resolved spectroscopy of dwarf planet (136472) Makemake. Astronomy and Astrophysics 577, A86

Mangold, N. 2011. Ice sublimation as a geomorphic process: A planetary perspective. Geomorphology 126, 1-17.

McKinnon, W. B. and A. C. Leith 1995. Gas drag and the orbital evolution of a captured Triton.. Icarus 118, 392-413.

Merlin, F., A. Alvarez-Candal, A. Delsanti, S. Fornasier, M. A. Barucci, F. E. DeMeo, C. de Bergh, A. Doressoundiram, E. Quirico, and B. Schmitt 2009. Stratification of Methane Ice on Eris' Surface. The Astronomical Journal 137, 315-328.

Millis, R. L., and 31 colleagues 1993. Pluto's radius and atmosphere - Results from the entire 9 June 1988 occultation data set. Icarus 105, 282

Moore, J. M. and J. R. Spencer 1990. Koyaanismuuyaw: The hypothesis of a perennially dichotomous Triton. Geophysical Research Letters 17, 1757-1760.

Moore, and 153 colleagues 2016. The geology of Pluto and Charon through the eyes of New Horizons. Science 351, 1284-1293.

Olkin, C. B., and 19 colleagues 1997. The Thermal Structure of Triton's Atmosphere: Results from the 1993 and 1995 Occultations. Icarus 129, 178-201.

Olkin, C. B., and 23 colleagues 2015. Evidence that Pluto's atmosphere does not collapse from occultations including the 2013 May 04 event. Icarus 246, 220-225.

Ortiz, J. L., and 55 colleagues 2012. Albedo and atmospheric constraints of dwarf planet Makemake from a stellar occultation. Nature 491, 566-569.

Ortiz, J. L., and 92 colleagues 2017. The size, shape, density and ring of the dwarf planet Haumea from a stellar occultation. Nature 550, 219-223.

Pál, A., C. Kiss, T. G. Müller, L. Molnár, R. Szabó, G. M. Szabó, K. Sárneczky, and L. L. Kiss 2016. Large Size and Slow Rotation of the Trans-Neptunian Object (225088) 2007 OR_{10} Discovered from Herschel and K2 Observations. The Astronomical Journal 151, 117.

Parker, and 15 colleagues 2016. Physical Characterization of TNOs with the James Webb Space Telescope. Publications of the Astronomical Society of the Pacific 128, 018010.

Pasachoff, J. M., and 14 colleagues 2017. Pluto occultation on 2015 June 29 UTC with central flash and atmospheric spikes just before the New Horizons flyby. Icarus 296, 305-314.

Perna, D., T. Hromakina, F. Merlin, S. Ieva, S. Fornasier, I. Belskaya, and E. Mazzotta Epifani 2017. The very homogeneous surface of the dwarf planet Makemake. Monthly Notices of the Royal Astronomical Society 466, 3594-3599.

Protopapa, and 22 colleagues 2017.Pluto's global surface composition through pixel-by-pixel Hapke modeling of New Horizons Ralph/LEISA data. Icarus 287, 218-228.

Quirico, E. and B. Schmitt 1997. Near-Infrared Spectroscopy of Simple Hydrocarbons and Carbon Oxides Diluted in Solid N ₂and as Pure Ices: Implications for Triton and Pluto. Icarus 127, 354-378.

Quirico, E., S. Douté, B. Schmitt, C. de Bergh, D. P. Cruikshank, T. C. Owen, T. R. Geballe, and T. L. Roush 1999. Composition, Physical State, and Distribution of Ices at the Surface of Triton. Icarus 139, 159-178.

Rossi, G. B., B. Sicardy, F. Braga-Ribas, R. Vieira Martins, J. Camargo, and M. Assafin 2014. The Use of Stellar Occultations to Study Trans-Neptunian Objects. AAS/Division for Planetary Sciences Meeting Abstracts #46 46, 510.09.

Rossi, G., R. Vieira-Martins, B. Sicardy, J. L. Ortiz and L. S. O. T. Rio Group 2017. Stellar Occultations by TNOs and Centaurs: first results in the “Gaia era”. AAS/Division for Planetary Sciences Meeting Abstracts #49 504.09.

Santos-Sanz, P. 2017. Physical characterization of Kuiper belt objects from stellar occultations and thermal measurements. European Planetary Science Congress 11, EPSC2017-97.
Schaller, E. L. and M. E. Brown 2007a.Volatile loss and retention on Kuiper Belt Objects. The Astrophysical Journal 659, L61-L64.
Schaller, E. L. and M. E. Brown 2007b. Detection of methane on Kuiper Belt Object (50000) Quaoar. The Astrophysical Journal 670, L49-L51.
Schmitt, and 28 colleagues 2017.Physical state and distribution of materials at the surface of Pluto from New Horizons LEISA imaging spectrometer. Icarus 287, 229-260.
Shinoda, T., 1969. Vapor pressure of carbon monoxide in condensed phases. Bull. Chem. Soc. Japan 42, 1815–1820.
Sicardy, B., and 23 colleagues 1999. The Structure of Titan's Stratosphere from the 28 Sgr Occultation. Icarus 142, 357-390.
Sicardy, B., and 40 colleagues 2003. Large changes in Pluto's atmosphere as revealed by recent stellar occultations. Nature 424, 168-170.
Sicardy, B., and 34 colleagues 2010. The 2010, February 19 stellar occultation by Varuna. Bulletin of the American Astronomical Society 42, 23.11.
Sicardy, B., and 61 colleagues 2011. A Pluto-like radius and a high albedo for the dwarf planet Eris from an occultation. Nature 478, 493-496.
Sicardy, B., and 67 colleagues 2016. Pluto's Atmosphere from the 2015 June 29 Ground-based Stellar Occultation at the Time of the New Horizons Flyby. The Astrophysical Journal 819, L38
Spencer, J. R., J. A. Stansberry, L. M. Trafton, E. F. Young, R. P. Binzel, and S. K. Croft 1997. Volatile Transport, Seasonal Cycles, and Atmospheric Dynamics on Pluto. Pluto and Charon 435.
Spencer, J. R., W. M. Grundy, F. Nimmo, L. A. Young. The Pluto system after New Horizons. This volume.
Stern, S. A. and L. M. Trafton 2008. On the Atmospheres of Objects in the Kuiper Belt. The Solar System Beyond Neptune 365-380.
Stern, S. A., and 14 colleagues 2017. New Horizons constraints on Charon's present day atmosphere. Icarus 287, 124-130.
Tan, S. P. and J. S. Kargel 2018. Solid-phase equilibria on Pluto's surface. Monthly Notices of the Royal Astronomical Society 474, 4254-4263.
Tegler, S. C., W. M. Grundy, W. Romanishin, G. J. Consolmagno, K. Mogren and F. Vilas 2007. Optical Spectroscopy of the Large Kuiper Belt Objects 136472 (2005 FY9) and 136108 (2003 EL61). The Astronomical Journal 133, 526-530.
Tegler, S. C., W. M. Grundy, F. Vilas, W. Romanishin, D. M. Cornelison and G. J. Consolmagno 2008. Evidence of N_2-ice on the surface of the icy dwarf planet 136472 (2005 FY9). Icarus 195, 844-850.
Tegler, S. C., W. M. Grundy, C. B. Olkin, L. A. Young, W. Romanishin, D. M. Cornelison, and R. Khodadadkouchaki 2012. Ice Mineralogy across and into the Surfaces of Pluto, Triton, and Eris. The Astrophysical Journal 751, 76.
Tickner, A.W., Lossing, F.P., 1951. The measurement of low vapor pressures by means of a mass spectrometer. J. Phys. Chem. 55 (5), 733–740.
Trafton, L. 1984. Large seasonal variations in Triton's atmosphere. Icarus 58, 312-324.

Trafton, L. M. 2015. On the state of methane and nitrogen ice on Pluto and Triton: Implications of the binary phase diagram. Icarus 246, 197-205.

Trafton, L. M., D. L. Matson, and J. A. Stansberry 1998. Surface/atmosphere Interactions and Volatile Transport (triton, Pluto and Io). In *Solar System Ices*, p. 773.

Trujillo, C. A., M. E. Brown, D. L. Rabinowitz and T. R. Geballe 2005. Near-Infrared surface properties of the two intrinsically brightest minor planets: (90377) Sedna and (90482) Orcus. The Astrophysical Journal 627, 1057-1065.

Trujillo, C. A., S. S. Sheppard, and E. L. Schaller 2011. A Photometric System for Detection of Water and Methane Ices on Kuiper Belt Objects. The Astrophysical Journal 730, 105

Tucker, O. J., J. T. Erwin, J. I. Deighan, A. N. Volkov, and R. E. Johnson 2012. Thermally driven escape from Pluto's atmosphere: A combined fluid/kinetic model. Icarus 217, 408-415.

Volkov, A. N., R. E. Johnson, O. J. Tucker and J. T. Erwin 2011a. Thermally Driven Atmospheric Escape: Transition from Hydrodynamic to Jeans Escape. The Astrophysical Journal 729, L24.

Volkov, A. N., O. J. Tucker, J. T. Erwin and R. E. Johnson 2011b. Kinetic simulations of thermal escape from a single component atmosphere. Physics of Fluids 23, 066601-066601-16.

Walker, A. C., C. H. Moore, D. B. Goldstein, P. L. Varghese, and L. M. Trafton 2012. A parametric study of Io's thermophysical surface properties and subsequent numerical atmospheric simulations based on the best fit parameters. Icarus 220, 225-253.

Wong, M. C. and W. H. Smyth 2000. Model Calculations for Io's Atmosphere at Eastern and Western Elongations. Icarus 146, 60-74.

Yelle, R. V. and J. I. Lunine 1989. Evidence for a molecule heavier than methane in the atmosphere of Pluto. Nature 339, 288-290.

Yelle, R. V., J. I. Lunine, J. B. Pollack, and R. H. Brown 1995. Lower atmospheric structure and surface-atmosphere interactions on Triton. Neptune and Triton 1031-1105.

Young, E. F. 1993. An Albedo Map and Frost Model of Pluto. Ph.D. Thesis.

Young, L. A. 2012. Volatile transport on inhomogeneous surfaces: I - Analytic expressions, with application to Pluto's day. Icarus 221, 80-88.

Young, L. A. 2013. Pluto's Seasons: New Predictions for New Horizons. The Astrophysical Journal 766, L22

Young, L. A. 2017. Volatile transport on inhomogeneous surfaces: II. Numerical calculations (VT3D). Icarus 284, 443-476.

Young, L. and W. B. McKinnon 2013. Atmospheres on Volatile-Bearing Kuiper Belt Objects. AAS/Division for Planetary Sciences Meeting Abstracts #45 45, 507.02.

Zhang, X., D. F. Strobel and H. Imanaka 2017. Haze heats Pluto's atmosphere yet explains its cold temperature. Nature 551, 352-355.

Zhu, X., D. F. Strobel, J. T. Erwin 2014. The density and thermal structure of Pluto's atmosphere and associated escape processes and rates. Icarus 228, 301–314.

Table 1. Volatile ices reported or suggested on Transneptunian Objects

Body	**CH_4 ice**	**N_2 ice**	**CO ice**
Triton	Multiple CH_4 bands directly detected	N_2 band directly detected. N_2-rich ice inferred from CH_4 band shifts.	Multiple CO bands directly detected
(134340) Pluto	Multiple CH_4 bands directly detected	N_2 band directly detected. N_2-rich ice inferred from CH_4 band shifts	Multiple CO bands directly detected
(136199) Eris	Multiple CH_4 bands directly detected	N_2-rich ice inferred from CH_4 band shifts	No spectral evidence.
(136472) Makemake	Multiple CH_4 bands directly detected	N_2-rich ice inferred from CH_4 band shifts	No spectral evidence.
(50000) Quaoar	Multiple CH_4 bands possibly directly detected	N_2 band possibly directly detected. N_2-rich ice inferred from CH_4 band shifts	No spectral evidence.
(225088) 2007 OR_{10}	CH_4 inferred by analogy with Quaoar.	No spectral evidence.	No spectral evidence.
(90377) Sedna	Possible absorption longward of 2.2 μm.	N_2 band possibly directly detected.	No spectral evidence.
(20000) Varuna	Possible absorption longward at 2.3 μm; more work is needed.	No spectral evidence.	No spectral evidence.
(90482) Orcus	Possible absorption at 2.2 μm.	No spectral evidence.	No spectral evidence.

Table 2. Results on atmospheres from stellar occultations

Name	Equivalent radius (km)	Surface Pressure	Reference
Triton	1350	3 - 11 μbar	Elliot et al. 2000
Pluto	1188	4 - 12.7 μbar	Sicardy et al. 2016
Eris	1163	< 1 nbar[a]	Sicardy et al. 2011
Haumea	816	< 10 nbar[a]	Ortiz et al. 2017
Makemake	715	< 12 nbar[a]	Ortiz et al. 2012
Charon	606	< 1.4 nbar[a]	Stern et al. 2017
Quaoar	555	< 21 nbar[a]	Braga-Ribas et al. 2013
Sedna	445	Inconclusive	Braga-Ribas et al. 2014b

[a] 1-σ upper limits.

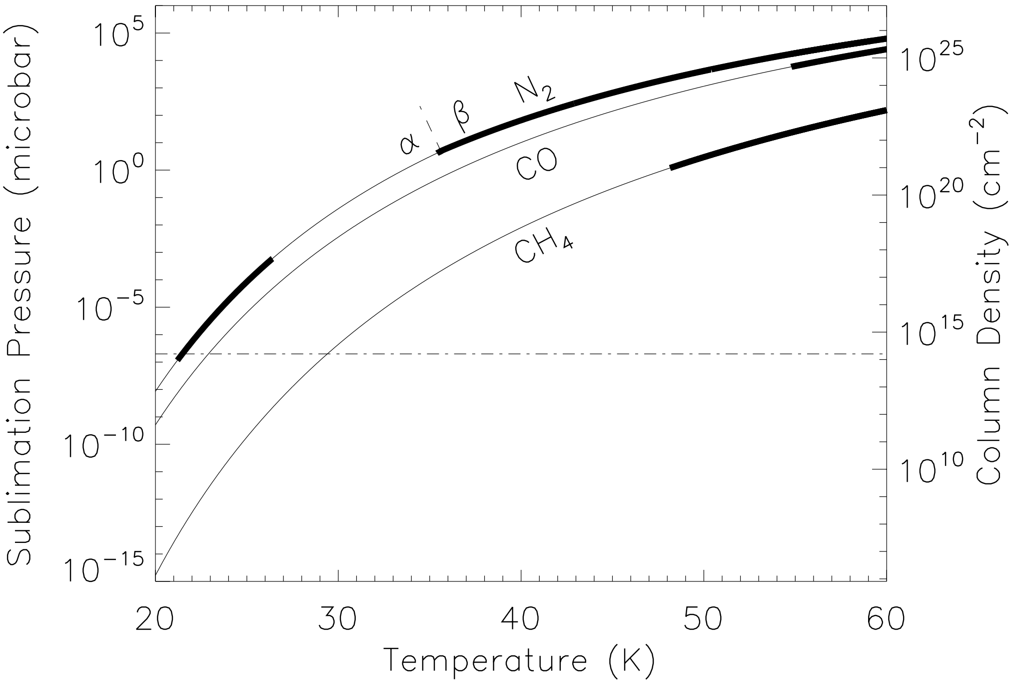

Fig. 1. Sublimation pressure (left axis) for N_2, CO, and CH_4 (Fray & Schmitt 2009; FS09). The column density (right axis) is calculated for a body with bulk density ρ of 1.9 g cm^{-3} and a surface radius r_0 of 500 km (N_2 or CO) or 875 km (CH_4); for a given pressure, the column density scales as 1/(ρ r_0). Thick lines show the ranges of temperatures at or below 60 K from laboratory measurements included in FS09: for N_2, 21.20-26.40 K (Borovik et al. 1960), 35.40-59.17 K (Frels et al. 1974), and 54.78–61.70 K (Giauque & Clayton 1933); for CO, 54.78–68.07 (Shinoda 1969); and for CH_4, 48.15–77.65 K (Tickner & Lossing 1951) and 53.15–90.66 K (Armstrong et al. 1955). The α-β phase transition for N_2 is indicated (35.61 K). The dot-dashed line indicates the rough transition between ballistic and collisional atmospheres, for ρ = 1.9 g cm^{-3} and r_0= 500 km.

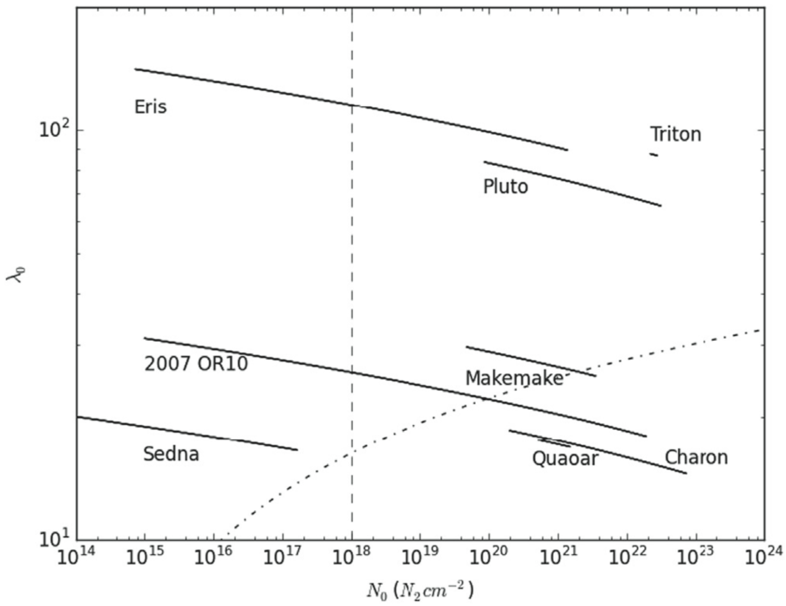

Fig. 2. Range of surface Jeans parameter, λ_0, vs. total column density, N_0, over the orbits of a number of TNOs assuming an N_2 atmosphere (Johnson et al. 2015) using ε = 0.8 and *A*=0.67, appropriate for an early TNO with a bright surface. For Makemake, 2007 OR_{10}, and Sedna we used ρ = 1.8 g cm^{-3}. Sedna's values are shown only near perihelion as its aphelion ($N_0 << 10^{14}$ cm^{-2}) is off-scale. Dashed line: $N_0 = 10^{18}$ N_2 cm^{-2}; to the right the CH_4 and N_2 components are sufficient so that escape is mainly driven by solar heating of the atmosphere. Dotted–dashed line: surface-heating-induced escape rate is smaller than Jean's formula below this line (warmer surface or lower surface gravity) and greater above this line. From Johnson et al. 2015. Reproduced by permission of the AAS.

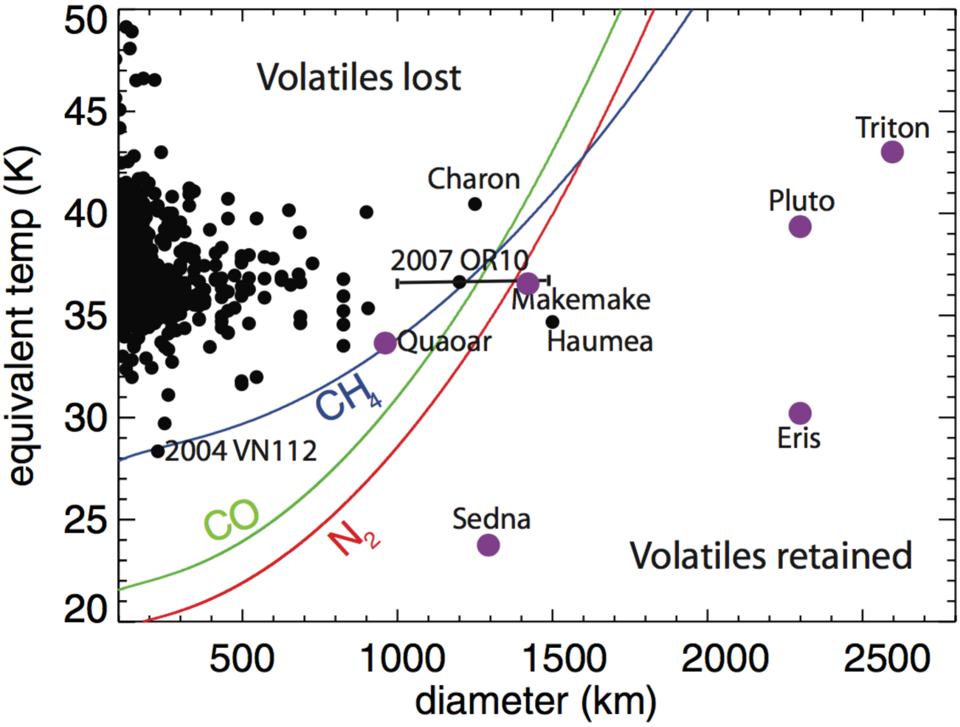

Figure 3. Plot of volatile retention and loss in the Kuiper belt, from Brown et al. 2011, updated from Schaller & Brown (2007b). Reproduced by permission of the AAS.

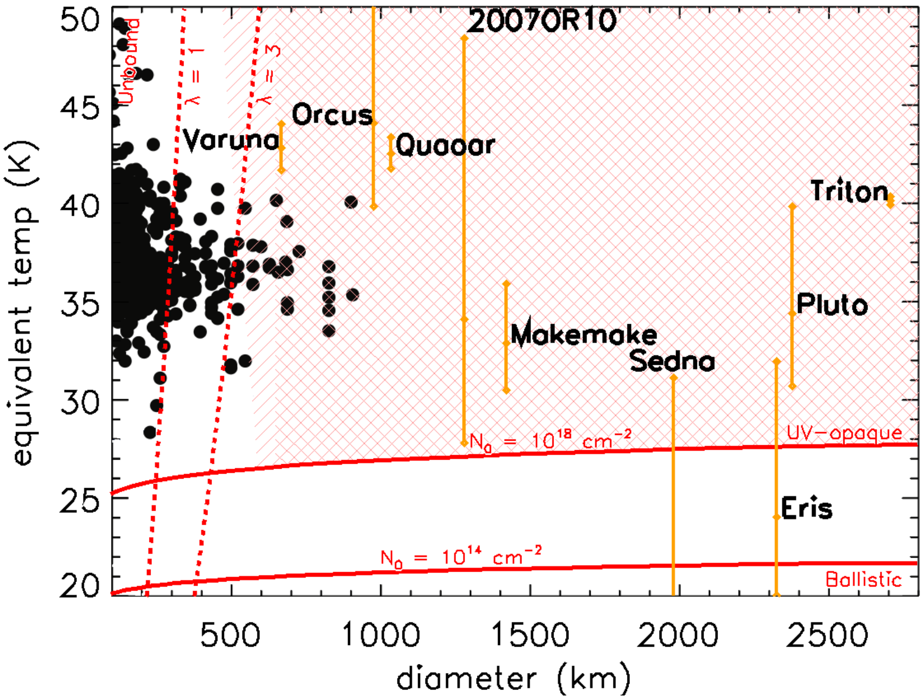

Figure 4. Diagram of escape regimes. Yellow: The nine bodies in Table 1 have been plotted: solid vertical lines show the variation in the average equilibrium temperatures between aphelion and perihelion (Eq. 1), using diameters and albedos from the tnosarecool database. Black: Diameters and temperatures taken from the retention plot of Brown et al. 2011. Solid red: Lines of constant column density at the surface for two critical values: for N_0 = 10^{14} cm^{-3} defining the classical surface-bounded exobase, and N_0 = 10^{18} cm^{-3} for an N_2 atmosphere with 3% CH_4 to be opaque to Ly-α. Dashed red: Lines of constant Jean's parameter for two critical values dividing the unbound and bound atmosphere (Volkov et al. 2011b). Hashed red: Atmospheric heating dominates the loss rate in the shaded region (adopted from the shaded regions in Fig 3 of Johnson et al. 2015) for A = 0.1 (single hash) and A = 0.67 (cross-hatched).

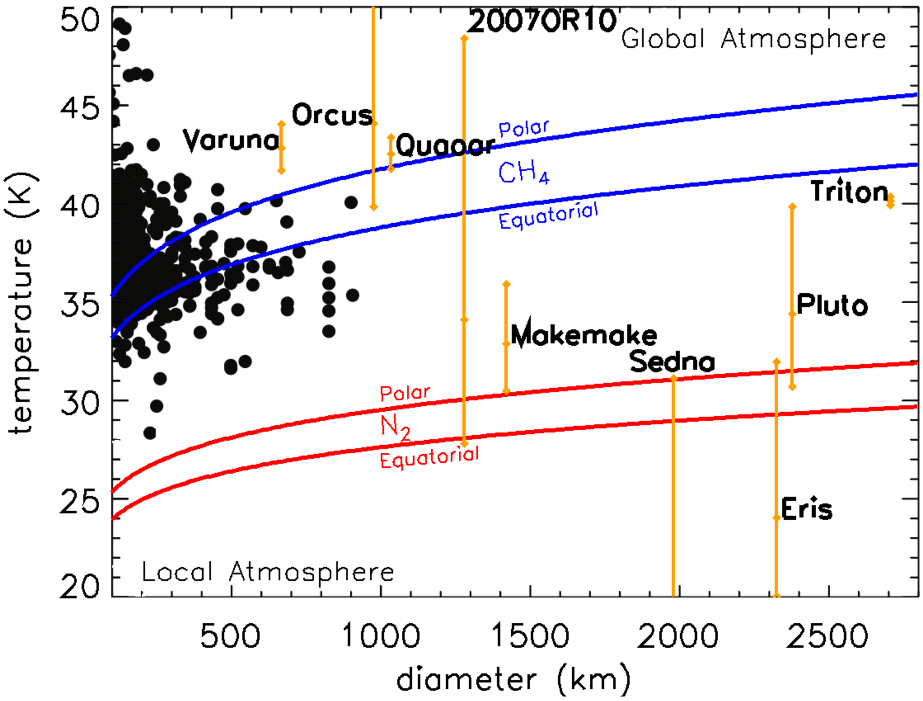

Figure 5. Minimum temperatures for a global atmosphere, assuming a surface uniformly covered with CH_4 ice (blue) or N_2 ice (red), for two extreme sub-solar latitudes. Several bodies would have global atmospheres at some portion of their orbit if covered with N_2 ice (Triton, Pluto, Eris, Makemake, and possibly Quaoar). A much smaller number of bodies would have global atmospheres at some portion of their orbit if covered with only CH_4 ice (possibly Varuna, Orcus, Quaoar, and 2007 OR10). Thermal inertia and non-uniform volatile ice coverage can change the range of temperatures actually achieved.

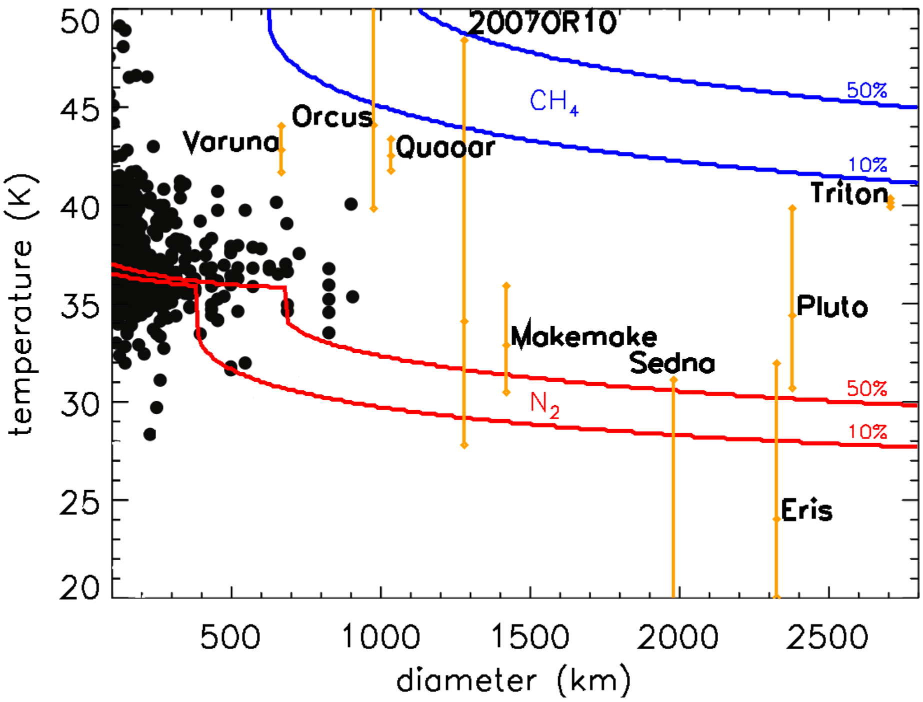

Figure 6. Detectability of TNO atmospheres by ground-based stellar occultation, under the assumption that the atmosphere is isothermal, and both atmosphere and surface are at the plotted temperature. The blue (CH_4) and red (N_2) detectability limits are for 50% or 10% drop in stellar flux for a surface-grazing ray.

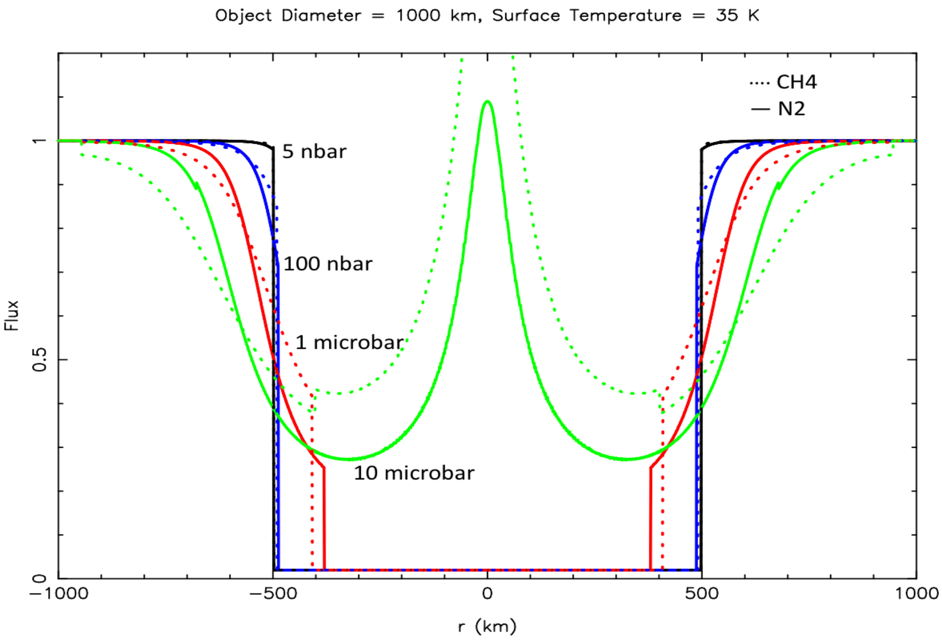

Figure 7: Synthetic light curve models of normalized stellar flux vs. shadow radius for an object with r_0 = 500 km, density 1.9 g cm^{-3}, Δ = 40 AU, with a surface temperature of T_0 = 35 K and a 5 K km-1 gradient to a 100 K upper atmosphere. Continuous lines are for an N_2-dominated atmosphere with surface pressures and column densities of p_0 = 0.005 μbar, N_0 = 4.0x10^{18} molecule cm^{-2} (black); 0.1 μbar, 8.1x10^{19} molecule cm^{-2} (blue); 1 μbar, 8.1x10^{20} molecule cm^{-2} (red), and 10 μbar, 8.1x10^{21} molecule cm^{-2} (green). Dashed lines are for a CH_4-dominated atmosphere with surface pressures and column densities of 0.005 μbar, 7.1x10^{18} molecule cm^{-2} (black); 0.1 μbar, 1.4x10^{20} molecule cm^{-2} (blue); 1 μbar, 1.4x10^{21} molecule cm^{-2} (red); and 10 μbar, 1.4x10^{22} molecule cm^{-2} (green).